International Journal of Solids and Structures 45 (2008) 4173–4183

Contents lists available at ScienceDirect

International Journal of Solids and Structures

journal homepage: www.elsevier.com/locate/ijsolstr

Mechanics of fluid-activated, clustered satellite bellows

James F. Wilson *

Department of Civil and Environmental Engineering, Pratt School of Engineering, Duke University, 6319 Mimosa Drive, Chapel Hill, NC 27514, United States

ARTICLE INFO

Article history:
Received 23 August 2007
Received in revised form 19 February 2008
Available online 12 March 2008

Keywords:
Actuators
Bellows
Corrugated tubes
Helical springs
Robotics

ABSTRACT

A bellows, or a closed thin-walled elastic tube with corrugated walls, undergoes longitudinal extension when subjected to internal fluid pressure. Investigated herein is the mechanical behavior of several pressurized bellows in clusters, which are designed to bend and twist as well as to extend and compress longitudinally. Bellows in clusters can be employed as robotic limbs, such as manipulator arms and legs for walking machines. For limb bending, analysis shows that there is an optimal geometry for satellite bellows, or a set of identical bellows clustered longitudinally about a central core. For limb torsion, the bellows are clustered in a cylindrical helix whose angle is chosen to produce the desired load–displacement relationships, for instance the highest rotation for a given torque. For both bending and torsional limbs, experimental results are included that exhibit the predicted mechanical behavior.

1. Introduction

The first important study involving mechanical behavior for single bellows was published by Donnell (1932). Subsequent surveys of the open literature on the subject were compiled by Mathney (1962) and evaluated by Wilson (1984a). Guidelines for bellows design using simplified analyses are found in EJMA (2003). Analyses of stiffness for multilayer rectangular corrugations were given by Reich et al. (2007) and for U-shapes by Wei-ping and Qian (2002). Analyses for static instability include those of Newland (1964) and Zhiming et al. (2003, 2002). Small vibrations of bellows, longitudinal and transverse, were addressed by Jakubauskas and Weaver (1996, 1998); and large dynamic behavior of bellows in bending were investigated by Wilson and Snyder (1989).

The use of bellows is widespread. Applications include descriptions of bellows for crushing in shock mitigation by Singace and El-Sobky (1997); bellows joints designed for hoses offshore by Witz et al. (2004); and bellows in strings and clusters for robotics by Pernette et al. (1997), Wilson and Mahajan (1989), and Wilson and Chen (1995). Investigations of bellows as related to the limbs and appendages of animals include the survey by Robinson and Davies (1999). Discussed in the three studies of Wilson et al. (1993, 1991), and Wilson (1984b), were the physical features and motion analyses for the elephant trunk and the squid tentacle. In these appendages, contractions of radial and circumferential muscles effect elongation, and contractions of selected longitudinal and helically wound muscle clusters produce bending and twisting, motions analogous to those of the pressurized bellows clusters discussed herein.

Shown in Fig. 1 is a concept design for a tapered, three-layered bellows-type fluid-actuated robotic limb. The limb is fixed at the larger diameter end, and the external loads are applied at the other (tip) end. The three layers are tightly packed around a flexible longitudinal core (a), which may be a bellows also. The inner layer consists of a longitudinally oriented satellite cluster (b), where six bellows were chosen for illustration purposes. When all of these inner layer bellows are pressurized equally, pure extension is realized. However, if only three of these adjacent bellows in this illustration are

* Tel.: +1 919 489 3041.
E-mail address: jwilson@duke.edu

0020-7683/$ - see front matter © 2008 Elsevier Ltd. All rights reserved.
doi:10.1016/j.ijsolstr.2008.02.027

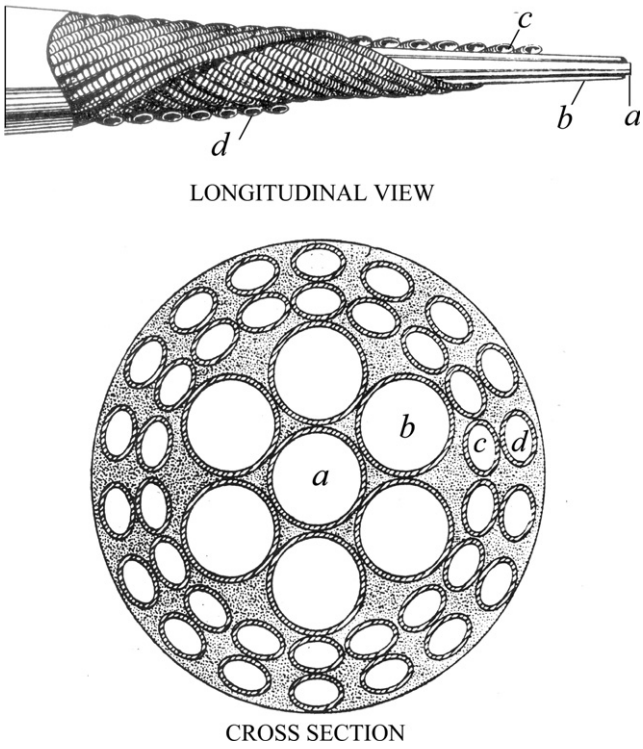

Fig. 1. A bellows limb, US Patent No. 4792173.

pressurized, the limb bends about a neutral axis coincident with the diametral line that separates the pressurized and unpressurized bellows.The middle layer (c) is a helically wound satellite cluster, as is the outer layer (d). However, the outer layer is wound in the opposite direction to the middle layer. When the bellows in middle layer are pressurized uniformly, the limb twists about the longitudinal axis; and when the bellows in the outer helical layer are pressurized, the limb twists in the opposite direction. Thus, the limb's tip motion, with or without tip loading, can be controlled by controlling the fluid pressure to selected bellows in the particular layers.

The main purposes of this paper are to present the mechanics or load-deformation analysis for two cases: limbs consisting of longitudinal and helically wound satellite clusters. In each case, experimental results are included that complement the analysis. The paper begins with a longitudinal case, in which the geometric arrangement is sought that maximizes the tip bending moment for selectively pressurized satellite bellows of a uniform limb. Following this is an analysis of the helical case, for which particular helical cluster angles for a uniform limb can be chosen to produce either the highest rotation or the highest torque. These separate studies form the bases for the design of optimal, multipurpose limbs such as depicted in Fig. 1.

2. Longitudinal bellows clusters

Shown in Fig. 2 is a typical cross-section of a uniform limb consisting of an even number of n identical closely packed longitudinal satellite bellows. The center of each bellows lies on a circle of radius a_0. Assume that $n/2$ adjacent satellite bellows are subject to the internal pressure p, which causes the cluster to bend about a neutral axis coincident to a diametral line precisely between the pressurized and unpressurized satellites. The pressure-induced bending moment is given by

$$M = p\pi R^2 \sum_{j=1}^{n/2} d_j \tag{1}$$

Here, R is the mean radius of a single satellite, defined in terms of its outer radius r_0 and the half-height of its corrugation h, or

$$R = r_0 - h \tag{2}$$

The moment arm for the jth satellite about the neutral axis is

$$d_j = a_0 \sin \alpha_j \tag{3}$$

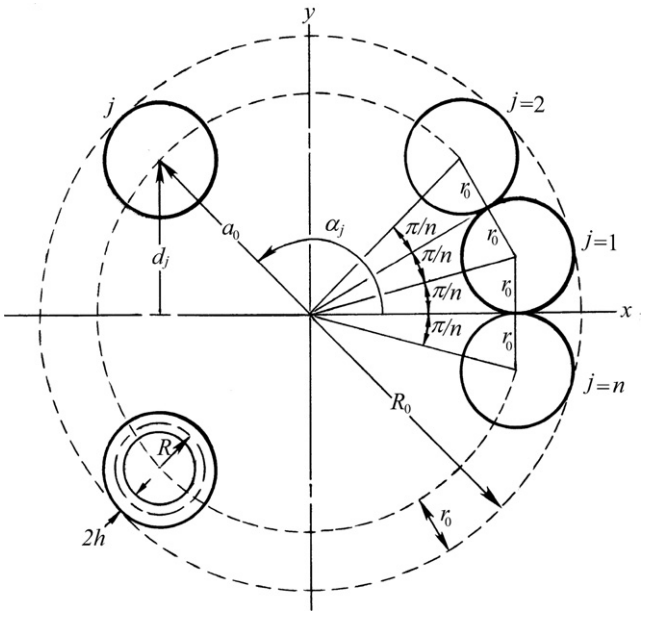

Fig. 2. Cross-section of a uniform limb with n satellite bellows, where n is an even number.

in which the center radius a_0 and the angle α_j of the jth satellite from the neutral bending axis are, respectively,

$$a_0 = \frac{r_0}{\sin \pi/n}; \quad \alpha_j = \pi(2j-1)/n \tag{4}$$

From Fig. 2, the geometric constraint relating r_0 to the whole cluster radius R_0 and the satellite angle π/n is

$$r_0 = (R_0 - r_0)\sin \pi/n \tag{5}$$

Introducing a constant C_n, then r_0 can be expressed as

$$r_0 = R_0 C_n; \quad C_n = \frac{\sin \pi/n}{1+\sin \pi/n} \tag{6}$$

With Eqs. (6) and (2), the moment given by Eq. (1) becomes

$$M = p\pi R_0^3 (C_n - h/R_0)^2 \sum_{j=1}^{n/2} d_j/R_0 \tag{7}$$

The term h/R_0 in the latter equation can be rewritten using Eqs. (2) and (6), or

$$\frac{h}{R_0} = \frac{h}{R}\frac{R}{R_0} = \frac{h}{R}\left(\frac{r_0}{R_0} - \frac{h}{R_0}\right) = \frac{h}{R}\left(C_n - \frac{h}{R_0}\right) \tag{8}$$

from which

$$\frac{h}{R_0} = \frac{C_n}{1+h/R} \tag{9}$$

With Eqs. (3), (4), (6) and (9), then Eq. (7) can be recast as the non-dimensional moment $\overline{M}$, defined by

$$\overline{M} = M\frac{(1+h/R)^2}{pR_0^3} = \frac{\pi \sin^2 \pi/n}{(1+\sin \pi/n)^3}\sum_{j=1}^{n/2} \sin[(2j-1)\pi/n] \tag{10}$$

Thus, for a fixed outer cluster radius R_0, given the satellite corrugation parameter h/R and the internal pressure p applied to $n/2$ adjacent bellows, the pressure-induced limb moment $\overline{M}$ is seen to depend only on n, an even number of compact satellite bellows.

Shown in Fig. 3 are the numerical results for $\overline{M}$, computed from Eq. (10) for even values of n. The peak moment, or $\overline{M} = 0.4654$, occurs for $n = 6$, which is defined as the optimal design configuration. For an increasing even $n > 6$, the moment $\overline{M}$ decreases monotonically with the shrinking radii of the satellite bellows. Computations show that the upper limit for real even values of n is 48, for which $\overline{M} = 0.1699$. Further, it is observed that the dimensional moment M, given fixed values for p, n, and R_0, varies as

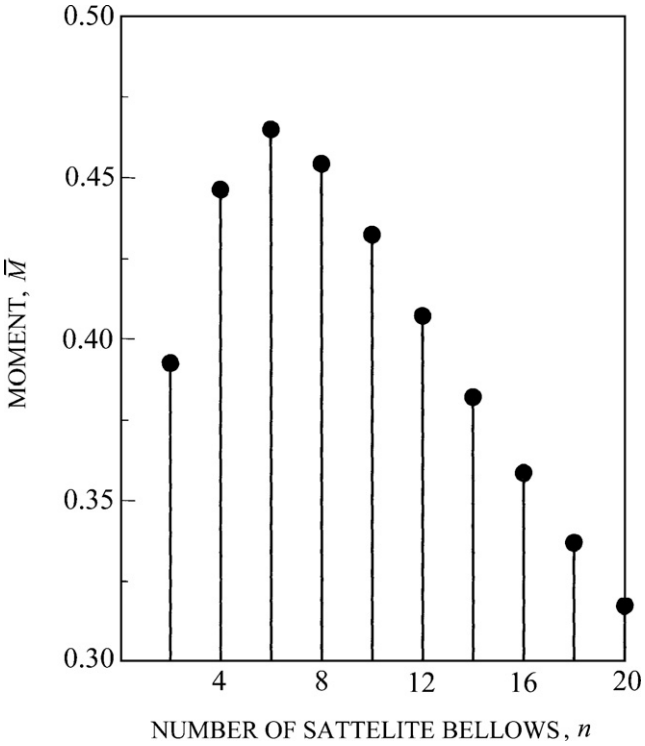

Fig. 3. Bending moment generated by pressurizing $n/2$ adjacent satellite bellows.

$$M \approx \frac{\text{const.}}{(1+h/R)^2} \tag{11}$$

which decreases rapidly as the corrugation depth ratio increases to its limit, $h/R \to 1$. The most striking result is that M increases as R_0^3, other parameters remaining the same. Thus, a doubling of the outside limb radius increases the limb's load-carrying capacity eightfold.

There are two other important observations gleaned from this analysis. First, for even n there are $n/2$ neutral axes for bending and thus there are $n/2$ principle directions of tip motion. Recall that the neutral axis is a diametral line dividing the $n/2$ pressurized and the $n/2$ unpressurized satellites. Second, for odd $n \geqslant 3$, the neutral axis of bending would bisect one of the satellite bellows, and that bisected bellows, if pressurized, would contribute nothing to the overall bending moment. Thus for odd n, one satellite would be a dummy and only $(n-1)/2$ pressurized satellites would contribute to the moment. It follows that even n produces the most efficient designs, and as shown in Fig. 3, $n = 6$ is the optimal one.

3. Bending of bellows in longitudinal clusters

A satellite bellows can be a monolithic tube with axially symmetric corrugations, such as the configurations discussed by Donnell (1932), Mathney (1962) and Wilson (1984a). Another type of bellows is a composite structure consisting of an elastic helical coil of spring steel embedded in a molded, closed corrugated tube. An example of the latter configuration is the hose of a household vacuum cleaner. A schematic view of this type of bellows is shown in Fig. 4, in which the geometric parameters $a,\ h,\ r_0,\ R$ and ℓ_0 are defined. Here, the polymeric material coating the steel helical spring has a negligible stiffness compared to that of the steel coil. Applied to the tip of the cantilevered coil is the axial load P_0 and the moment M_0. As discussed by Wahl (1944) and Timoshenko and Gere (1961), a suitable approximation to the transverse tip displacement under these loads is given by

$$\delta_0 = \frac{M_0 \ell_0^2}{2\beta_0} \frac{1}{1+P_0/P_c}; \quad P_c = \frac{\pi^2 \beta_0}{c\ell_0^2} \tag{12}$$

In Eq. (12), the bending stiffness β_0 is defined by

$$\beta_0 = \frac{2\ell_0 EIG}{m\pi R(2G+E)}; \quad I = \frac{\pi}{4}a^4 \tag{13}$$

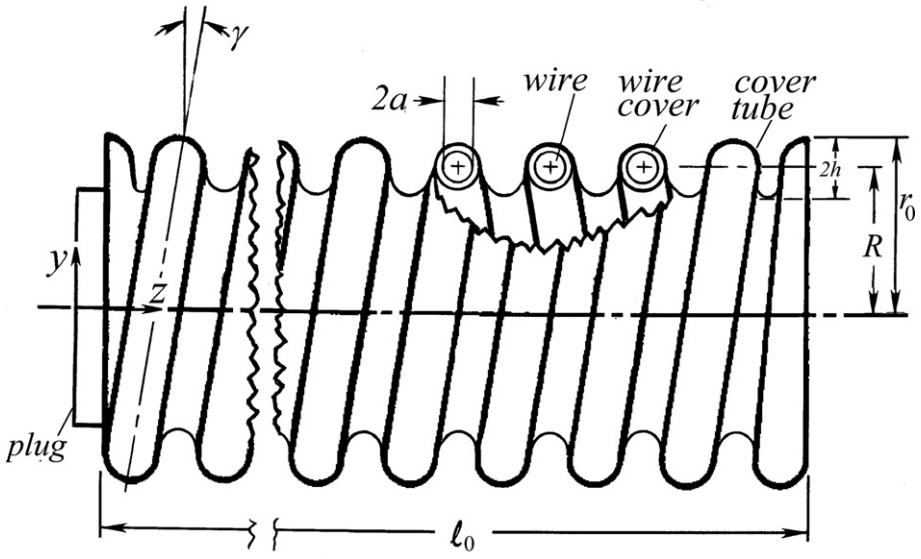

Fig. 4. Bellows formed of a steel helical spring imbedded in a polymeric material.

where E and G are Young's modulus and the shear modulus, respectively, for the helical coil and m is the number of coils. The term containing P_0/P_c accounts for the stretching of the longitudinal axis, which effects a reduction in the transverse deflection compared to that deflection caused by M_0 acting alone. The constant c in the denominator of the reference load P_c is in the range $1 \leqslant c \leqslant 4$, in which the lower and upper limits represent a hinged end and a clamped end, respectively. In practice, neither fixity condition can be realized. Experimental evidence presented later shows that c for practical cases is generally in the midrange of these extremes for helical springs.

Donnell (1932) assumed that a monolithic corrugated tube in bending can be modeled as a smooth tube with a reduced, equivalent bending stiffness. Based on this same reasoning, then the equivalent bending stiffness for the helical spring of Fig. 4 can be defined as

$$E_e I_e = \frac{2\ell_0 EIG}{m\pi R(2G+E)} \tag{14}$$

in which the equivalent modulus and area moment of inertia for the smooth tube are

$$E_e = \frac{EG}{2G+E} \tag{15}$$

$$I_e = \pi R^3 t = \frac{\ell_0 a^4}{2mR} \tag{16}$$

From this last result, the thickness of the equivalent thin-walled tube is deduced as

$$t = \frac{\ell_0 a^4}{2m\pi R^4} \tag{17}$$

The calculation of the transverse tip displacement δ_0 of a cantilevered limb cluster for $n = 6$ identical satellite tubes, half of which are pressurized, is illustrated for two cases. In the first case, assume that the unpressurized core tube is identical to the other six and that all tubes are glued or welded together at every point of contact so that the limb cluster acts as a single unit under transverse bending. When the parallel axis theorem is applied to the seven tubes, an upper bound value for the area moment of inertia about the neutral axis of bending is calculated as

$$I_e = 31\pi r_0^3 t \tag{18}$$

In the second case, assume that all points of contacts between adjacent tubes are frictionless so that each tube acts independently during transverse bending. This leads to the following lower bound value for I_e, or

$$I_e = 7\pi r_0^3 t \tag{19}$$

Given the limb's total tip loading M_t and P_t, Eq. (12) can be recast in terms of the tube limb cluster parameters to give the transverse tip displacement for $n = 6$ as

$$\delta_0 = \frac{M_t \ell_0^2}{2E_e I_e} \frac{1}{(1 + P_t/P_c)}; \quad P_c = \frac{\pi^2 E_e I_e}{c\ell_0^2} \tag{20}$$

Here, E_e and t are given by Eqs. (15) and (17), and a lower and upper bound for δ_0 can be computed by using I_e Eq. (18) or (19), respectively. The end fixity parameter c is determined experimentally.

For the special case in which all bellows of the limb are subjected to the same internal pressure p, the transverse bending is zero and the axial extension δ is the same for each of the bellows. For an enclosed helical coil or bellows with an axial load of $P = \pi R^2 p$, the axial extension derived by Wahl (1944) is given by

$$\delta = \frac{4\pi R^5 mp}{Ga^4} \tag{21}$$

in which R is the mean radius of the coil, a is the imbedded wire radius and m is the number of coils in one bellows.

4. Experiments on an extension and bending limb

Shown in Fig. 5 is a uniform experimental limb designed for extension and bending. It is composed of seven identical bellows of the type described in Fig. 4. The assembly is held together with epoxy cement at the points of bellows contact and thin strings are wrapped around the whole circumference. Its design parameters, defined in Figs. 4 and 5, are: a = 0.60 mm, h = 2.17 mm, $\ell_0 = 215$ mm, $r_0 = 17.1$ mm, R = 14.93 mm, $\gamma = 8.5°$, E = 207 GPa, G = 79.3 GPa, m = 63, and n = 6.

This limb is an optimal six-satellite design that extends uniformly when all bellows are pressurized equally, and bends about its rigid base when three of the six adjacent satellites are pressurized. Each bellows has its own air pressure supply line connected from its base port to a control module. The electronic interfaces between the pressure control module and the computer that allow for software control of the pulsed air supplied to each tube are described in detail by Wilson et al. (1993).

In the first series of experiments, equal internal pressure was applied to all seven bellows tubes and the extension was measured with a micrometer. These data shown in Fig. 6 suggest non-linear hardening, which is caused by the tendency of

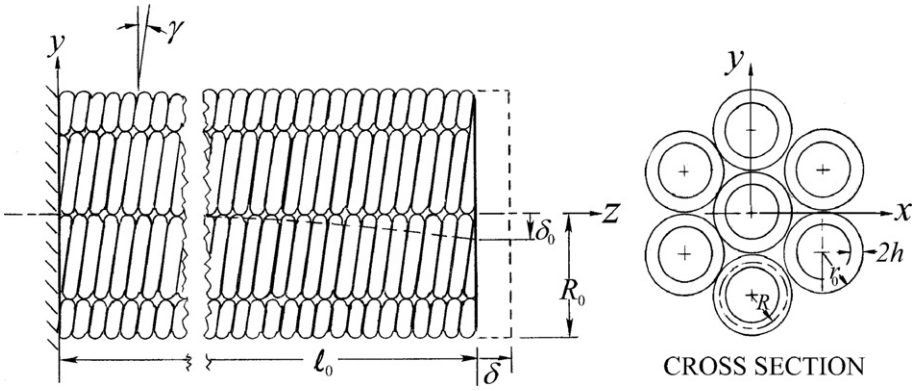

Fig. 5. Design of the optimal experimental bending limb.

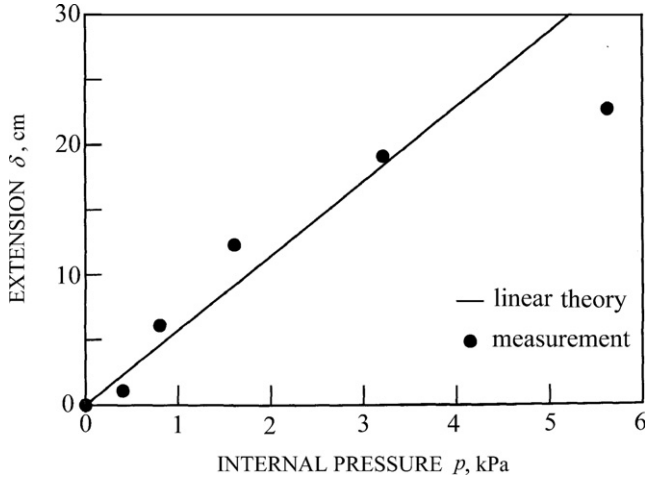

Fig. 6. Uniform extension of the optimal bending limb, with all seven bellows pressurized equally.

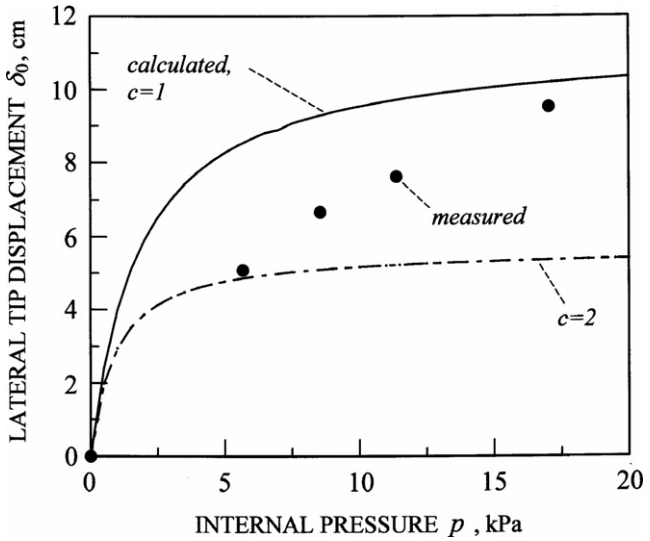

Fig. 7. Lateral tip displacement of the optimal bending limb, in which only three adjacent satellite bellows are pressurized.

the bellows to straighten and the corrugations to flatten with increasing pressure p. The first data point is an exception to this trend, where its low extension may be due to one or both of the following factors: an error in reading the micrometer, or an enhanced initial limb stiffness due to some initial stick friction between adjacent the bellows. Also shown in Fig. 6 is the theoretical relationship between the longitudinal extension and the internal pressure p, as predicted by Eq. (21). For this limb, that relationship is $\delta = 5.72p$, in which the units of deflection and pressure are cm and kPa, respectively. It is observed that the theory is in best agreement with the data for longitudinal limb strains of up to 80%.

In the second series of experiments, an internal pressure p was imposed on three adjacent satellite bellows and the limb's lateral tip deflection δ_0 was measured with a micrometer. These data are shown as circles in Fig. 7. For these three active bellows, the loadings were based on the bellows constants listed in the first paragraph of this section. These loadings were $P_t = 3\pi R^2 p$ and $M_t = 4\pi R^2 r_0 p$. Also, E_e and t were computed from Eqs. (15) and (17). The theoretical lower and upper bound curves for δ_0 as a function of pressure p were computed from Eq. (20), using I_e defined by Eq. (18). Chosen for a lower bound curve was $c = 2$, a boundary constraint between the fully clamped condition $c = 4$ and the frictionless hinged condition $c = 1$. Chosen for the upper bound curve was $c = 1$. One interpretation of the experimental data and theoretical results in Fig. 7 is that as the pressure increases the partially clamped end loosens and the end fixity approaches that of a hinged end. Another interpretation is that the limb undergoes hardening because the bellows tend to straighten and the corrugations tend to flatten with increasing pressure p, as was observed for the single bellows in Fig. 6. Both factors may contribute to the experimental behavior shown in Fig. 7.

5. Torsion of bellows in helical clusters

Shown in Fig. 8 is a photograph of the experimental torsional limb. Torsion is achieved by pressurizing the six tightly packed satellite bellows, held together with epoxy cement at the tips of their corrugations, and oriented to form a cylindrical helix. This design has a constant cylindrical helix angle of $\alpha = 53^\circ$ relative to the transverse axis. As predicted by Wilson and Orgill (1986), this helix angle produces the maximum twist angle for a given internal pressure, other design parameters remaining the same. Although their result was derived for a thin-walled orthotropic cylinder with its weaker axis inclined at $\alpha = 53$, such a result is appropriate for the present case as well. If a high torque and low rotation were desired, then α would be about 70°, as predicted by Wilson and Orgill (1986). In the experimental setup, the six-bellows unit of Fig. 8 is affixed to a rigid base through which passes an air supply line to each bellows. The unit is clamped around an aluminum disc at the tip. Fixed above the tip in the horizontal plane is a protractor (not shown), which is used to measure limb rotation.

The bellows of this experimental limb were made of neoprene-latex rubber and are commercially available as boots for mechanical equipment. These bellows differed from those previously used in the bending limb in that the corrugations were axially symmetric and the structure was monolithic, i.e. no wire reinforcement. One of the six-bellows employed in the experimental limb is depicted in Fig. 9 and its geometric parameters are: $4b = 7.71$ mm, $2h = 4.2$ mm, $\ell_0 = 280$ mm, $R = 5.56$ mm, $t = 0.85$ mm.

The apparent modulus of elasticity E' in extension for the single bellows shown in Fig. 9 was empirically determined by applying a range of axial loads P and measuring the corresponding axial extension $\Delta\ell_e$. Then E' was computed using linear regression, a least-squares fit of the $(P, \Delta\ell_e)$ data to the one dimensional stress–strain relationship, or

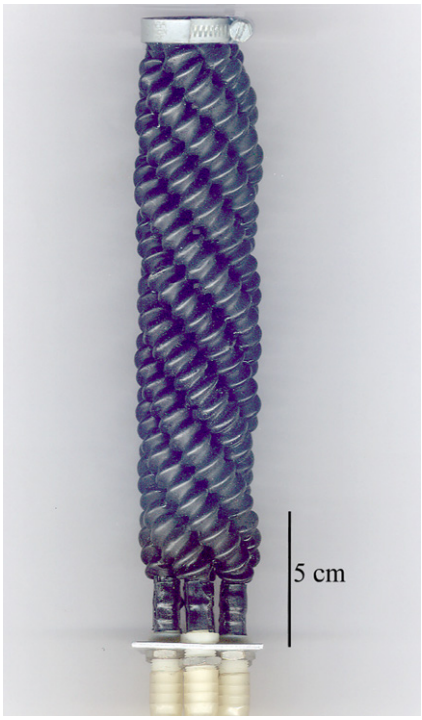

Fig. 8. The experimental torsional limb made of six monolithic neoprene-latex bellows closely packed in a cylindrical helix.

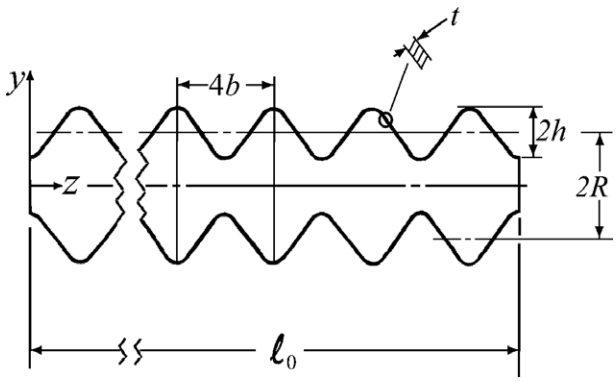

Fig. 9. Outline of a thin-walled neoprene-latex bellows used in a torsional limb.

$$\Delta\ell_e = \frac{P\ell_0}{(2\pi Rt)E'} \tag{22}$$

In Eq. (22), the axial load P is applied to the area $2\pi Rt$. Based on the thin wall approximation, this is the equivalent cross-section area of a solid tube of wall thickness t and mean radius R. The results gave

$$E' = 648 \text{ kPa} \tag{23}$$

for which the 95% confidence limits, low and high, were computed as 628 kPa and 668 kPa, respectively. These confidence limits were computed by the Pivotal Method, which is formulated and illustrated in great detail by Mendenhall and Sincich (1984).

Consider the schematic representations of the torsional limb shown in Fig. 10. Depicted on the left is the cylinder of radius $\overline{R}$, which is the radial distance between the centerline of the limb and the centerline of a satellite bellows. The cylindrical helix is the path followed by the centerline of a single bellows of length ℓ_0, a path that begins at the base point A, wraps around the cylinder, and terminates at the tip point B. For the experimental limb, the total winding angle θ from the base to the tip is equal to one and a half turns, or $\theta = 3\pi$. With internal pressure, ℓ_0 extends by $\Delta\ell$ and θ increases by $\Delta\theta$ as the

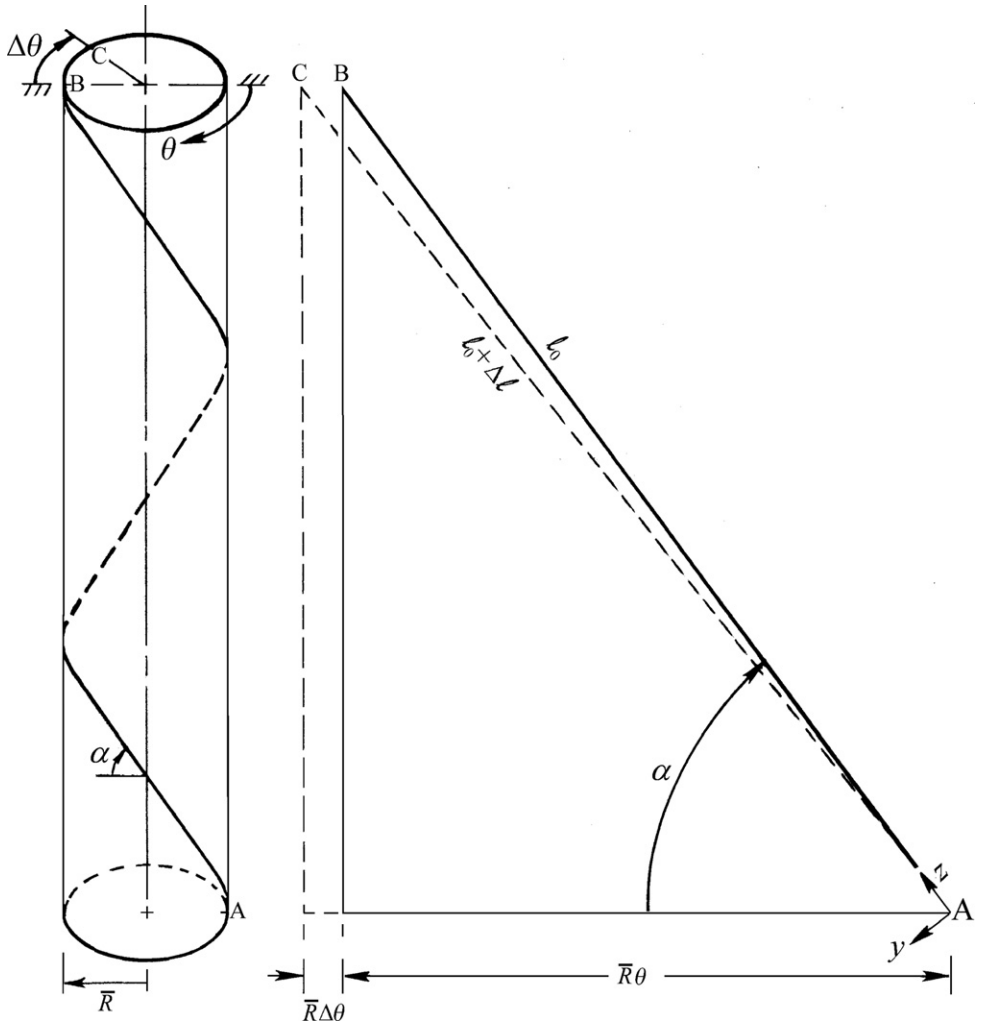

Fig. 10. Representations of the torsional limb: cylindrical helical path of the centerline for a single bellows (left); and a flat view of that single bellows (right).

tip point B rotates to C. The cylinder height is assumed to remain constant. It follows from the flat view of the cylinder shown on the right of Fig. 10 that

$$\overline{R}^2(\theta+\Delta\theta)^2 = (\ell_0+\Delta\ell)^2 - (\ell_0\sin\alpha)^2 \tag{24}$$

For each bellows that wraps around the cylinder, the length change can be expressed in the same form as Eq. (22), or

$$\Delta\ell = \frac{p\pi R^2\ell_0}{(2\pi Rt)eE'} = \frac{pR\ell_0}{2teE'} \tag{25}$$

Here, the mean bellows radius is R, the pressure load in each curved bellows is $p\pi R^2$ and the apparent modulus is defined as eE'. The constant $e > 1$, which is measured in a given application, accounts for the increase in E' over its value in pure extension, an increase due to bellows curvature and fixity of each bellows peak corrugation to its nearest neighbor. When Eqs. (24) and (25) are combined to eliminate $\Delta\ell$, and $\theta = (\ell_0/\overline{R})\cos\alpha$ is used, then the resulting equation can be solved for the change in the tip rotation angle due to pressure. Thus

$$\Delta\theta = \frac{\ell_0}{\overline{R}}\left[\left((1+\frac{pR}{2teE'}\right)^2 - \sin^2\alpha\right]^{1/2} - \frac{\ell_0}{\overline{R}}\cos\alpha \tag{26}$$

In the special case of small angles of rotation, it follows from the flat view of Fig. 10 that the change is bellows length can be approximated by

$$\Delta\ell \approx \overline{R}\Delta\theta\cos\alpha \tag{27}$$

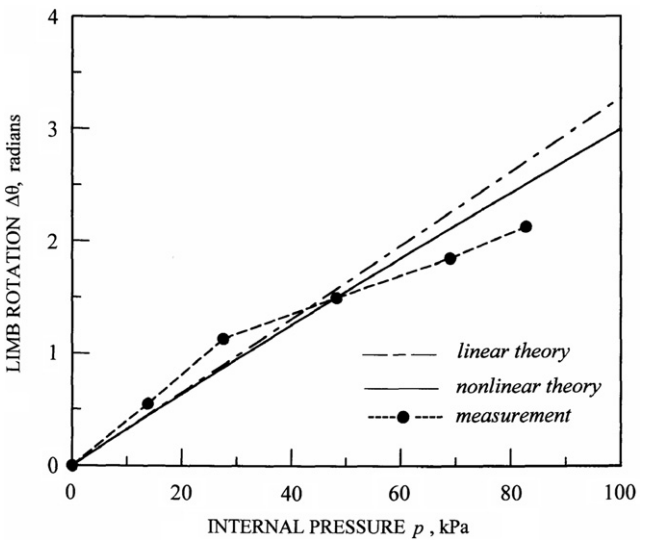

Fig. 11. Tip rotation of the experimental torsional limb with internal pressure.

With Eqs. (25) and (27), the small angle approximation then leads to the linear form

$$\Delta\theta \approx \frac{pR\ell_0}{2\bar{R}teE'\cos\alpha} \tag{28}$$

It is noted that the results of Eqs. (26) and (28) apply to both a single cylindrical helical bellows and to a tight cluster of several such bellows in the same geometric configuration.

Shown in Fig. 11 are the experimental and computed results for the rotation of the limb depicted in Fig. 8. The experimental data (black circles) appear bilinear with an increase in stiffness at about 29 kPa. This could come about if there were slip between adjacent bellows at the lower pressures p. However, the experimental bellows remained glued together, so that relative slip was doubtful. Suppose instead that these data follow (within experimental error) a smooth curve with non-linear hardening as observed for the limbs of Figs. 6 and 7, in which the corrugations tended to straighten and flatten with increasing pressure p. This latter interpretation is preferred for the torsional bellows.

The theoretical curves of Fig. 11 are based on dimensional parameters defined in Figs. 9 and 10: $\ell_0 = 280$ mm, $\bar{R} = 18.4$ mm, $\alpha = 0.923$ rad, $\theta = 3\pi$ rad. These values were used to compute the tip rotation $\Delta\theta$ of the experimental limb as a function of internal pressure p. It is seen that linear theory, Eq. (28), overpredicts $\Delta\theta$, as compared to the more exact non-linear theory, Eq. (26). In both theories, $e = 3.9$, which was deduced as the best-fit constant to the measurements obtained using the experimental limb. For this six-bellows limb, the apparent modulus in the direction of the helix is $eE' = (3.9)(648)$ kPa = 2.53 MPa. This latter result can be compared to Young's modulus of $E = 2.6$ MPa for a somewhat similar but uniform material: latex rubber (Gibson and Ashby, 1999).

6. Summary and conclusions

Through theory and experiment, it was found that uniform bellows can be clustered and oriented in particular ways to form actuator limbs. For instance, an optimal limb consisting of six-satellite bellows in a tight longitudinal cluster leads to the peak bending action when three adjacent bellows are pressurized. Also, a limb designed of six tightly clustered pressurized bellows oriented in a cylindrical helix produces rotation about the longitudinal axis. In this case, the helix angle producing peak rotation is predicted to be 53° with respect to the transverse limb axis. With pressure control, such limbs acting separately or in combination, mimic the muscle controlled action in the squid tentacle and the elephant trunk. Pressure-controlled limbs can be employed for use as robotic actuators, especially in applications for which robust action is favored over the precision of movement.

Acknowledgements

The experimental work, carefully performed by Neal Myerson and Andrew Feinberg, is gratefully acknowledged.

References

Donnell, L.H., 1932. The flexibility of corrugated pipes under longitudinal forces and bending. Journal of Applied Mechanics 69 (APM-54-7).
EJMA, 2003. Standards of the Expansion Joint Manufacturers Association, eighth ed. EJMA, Inc., Tarrytown, NY.

Gibson, L.J., Ashby, M.F., 1999. Cellular Solids: Structure and Properties, second ed. Cambridge University Press, Cambridge.
Jakubauskas, V.F., Weaver, D.S., 1996. Axial vibrations of fluid-filled bellows expansion joints. Journal of Pressure Vessel Technology 118, 484–490.
Jakubauskas, V.F., Weaver, D.S., 1998. Transverse vibrations of bellows expansion joints, part II: beam model development and experimental verification. Journal of Fluids and Structures 12 (4), 457–473.
Mathney, J.D., 1962. Bellows spring rate for seven typical convolution shapes. Machine Design 3, 137–138.
Mendenhall, W., Sincich, T., 1984. Statistics for the Engineering and Computer Sciences. Dellen, Santa Clara, California.
Newland, D.E., 1964. Buckling of double bellows expansion joints under internal pressure. Journal of Mechanical Engineering Science 6, 270–277.
Pernette, E., Henein, S., Magnani, I., Clavel, R., 1997. Design of parallel robots in microrobotics. Robotica 15, 417–420.
Reich, J., Cardella, A., Capriccioli, A., Koppe, T., Missal, B., Lohrer, W., Langone, S., Sassone, P.C., 2007. Experimental verification of the axial and lateral stiffness of large W7-X rectangular bellows. Fusion Engineering and Design 82, 1924–1928.
Robinson, G., Davies, J.B.C., 1999. Continuum robots – a state of the art. Robotics and Automation 4, 2849–2854.
Singace, A.A., El-Sobky, H., 1997. Behaviour of axially crushed corrugated tubes. International Journal of Mechanical Sciences 39 (3), 249–268.
Timoshenko, S.P., Gere, J.M., 1961. Theory of Elastic Stability. McGraw-Hill, New York.
Wahl, A.M., 1944. Mechanical Springs. Penton Publishing Co., Cleveland, OH.
Wei-ping, Z., Qian, H., 2002. General solution of the overall bending of flexible circular ring shells with moderately slender ratio and applications to the bellows (IV)-calculation for U-shaped bellows. Applied Mathematics and Mechanics 23, 1164–1169.
Wilson, J.F., 1984a. Mechanics of bellows: a critical survey. International Journal of Mechanical Science 26 (11/12), 593–605.
Wilson, J.F., 1984b. Robotic mechanics and animal morphology. In: Brady, M. (Ed.), Robotics and Artificial Intelligence, Computer and System Sciences, Series F, vol. II. Springer Verlag, Berlin, pp. 419–443.
Wilson, J.F., Chen, Z., 1995. A whisker probe system for the shape perception of solids. Journal of Dynamic Systems, Measurement, and Control 117 (1), 104–108.
Wilson, J.F., Li, D., Chen, Z., George, R.T., 1993. Flexible robot manipulators and grippers: relatives of elephant trunks and squid tentacles. In: Dario, P. (Ed.), Robots and Biological Systems: Towards a New Bionics? Springer Verlag, Berlin, pp. 475–494.
Wilson, J.F., Mahajan, U., 1989. The mechanics and positioning of highly flexible manipulator limbs. Journal of Mechanics, Transmissions and Automation in Design 111 (3), 230–237.
Wilson, J.F., Mahajan, U., Wainwright, S.A., Croner, L., 1991. A continuum model of elephant trunks. Journal of Biomechanical Engineering 113, 79–84.
Wilson, J.F., Orgill, G., 1986. Linear analysis of uniformly stressed, orthotropic cylindrical shells. Journal of Applied Mechanics 53, 249–256.
Wilson, J.F., Snyder, J.M., 1989. The elastica with end-load flip-over. Journal of Applied Mechanics 55, 845–848.
Witz, J.A., Ridolfi, M.V., Hall, G.A, 2004. Offshore LNG transfer – a new flexible cryogenic hose for dynamic service, OTC 16270. In: Proceedings of the Offshore Technology Conference, Houston, TX.
Zhiming, L., Jie, J., Zengliang, G., Yi, Q., 2003. Effects of axial deformation on in-plane instability of U-shaped bellows. Journal of Pressure Vessel Technology 125 (4), 475–477.
Zhiming, L., Shuiguang, T., Yi, Q., Deming, F., Zengliang, G., 2002. In-plane instability tests of bellows subjected to internal pressure and deformation load. International Journal of Pressure Vessels and Piping 79 (3), 245–247.